ISSN (Print) 1226-1750
ISSN (Online) 2233-6656
Journal of Magnetics 25(2), 269-276 (2020) https://doi.org/10.4283/JMAG.2020.25.2.269

Discussion of the Influence of Geometric Discontinuity and Stress Concentration on the Magnetic Memory Method

Gang Han and Haihong Huang*

School of Mechanical Engineering, Hefei University of Technology, Hefei, China

(Received 11 September 2019, Received in final form 26 May 2020, Accepted 3 June 2020)

In this study, a multi-physics finite element model is adopted to investigate the effect of geometric discontinuity and stress concentration on the magnetic memory method (MMM). We propose a quadratic equation to fit the stress magnetization constitutive relation in the model. The relation can be used to predict the abnormality of the geometric discontinuity and the stress concentration. Simulation results show that the magnetization on the wall of the groove is the weakest and that on the bottom of the groove is the maximum. The free boundary condition releases the stress concentration of the defect. Although the magnetization induced by stress concentration is weaker than geometric discontinuity, the signal characteristics can still be used to evaluate the defect and the stress. This work proves that the MMM is a potential method for stress distribution assessment.

Keywords : magnetic memory method (MMM), magnetostriction, stress concentration

1. Introduction

As a comparative novel non-destructive testing (NDT) method, the magnetic memory method (MMM) is the only potential NDT technology for evaluating stress concentration [1]. Thus, the MMM is widely used in various industries, such as rails, pipelines, and weld structures [2, 3], to diagnose the early damage of the structure.

This method is regarded as a passive magnetic flux leakage (MFL) method, and spontaneous magnetization results from the magneto mechanical (Villari) effect. However, many factors determine the Villari effect [4-7], including the geomagnetic field, the initial stress state, the chemical composition, the microstructure, the geometry, and the dimension of samples. Many experiments have been carried out to clarify the relationship between all these factors and the self-magnetic leakage field (SMLF). Various defects were prefabricated to induce local stress concentration, and then the distribution of the SMLF induced by stress was measured [8-10]. The magnetic signals are the result of the combined effect of geometric discontinuity, stress concentration, and other factors [11]. In published literature, since the geomagnetic field, initial magnetic state, and chemical composition of samples are known in advance, the geometric discontinuity and the stress concentration are the main factors that determine the leakage of the magnetic field.

Some researchers focused on the effect of geometric discontinuity [12]. Wang and Yao *et al.* [13] investigated the distribution of MMM signals based on the magnetic charge theory. Later, they performed a 3D finite element (FE) analysis to capture the circular and square plastic zones by calculating the MMM signals of the specimen [14]. They just considered the specimen as a permanent magnet and ignored the non-uniform magnetization caused by the stress concentration. However, the magnetization induced by stress is non-uniform, which is very different from the traditional MFL method.

On the other hand, some researchers claimed to have found a direct relationship between residual stress and the magnetic field gradient [15]. Other studies [16] reconstructed the experiment and proved that a bidirectional correlation between the magnetic field gradient and the local stress level cannot be determined because of several inseparable factors. These contradictory statements indicate that the mechanism of the MMM has not been satisfactorily investigated [1].

As a static harmonic field, the magnetic field distribution is mainly determined by Maxwell's equations and the

*Corresponding author: Tel: +86-0551-62901351
Fax: +86-0551-62901351, e-mail: huanghaihong@hfut.edu.cn

constitutive relation. Establishing the quantitative relationship between the shape and size of the defect and the magnetic signals is the key issue of the MMM. Several models, such as the Jiles–Atherton (J–A), Preisach, and Hauser models, can predict the magnetization behavior quantitatively based on a solution of nonlinear differential equations [17, 18]. Shi [19] proposed a nonlinear constitutive relation of the magneto mechanical model and conducted a study with new findings of the applicability of the MMM. The results of the improved model are consistent with the experimental data and demonstrate its feasibility for early diagnosis. The model can clarify some complex phenomena of the MMM signals [20].

However, in practical applications, the environment around a specimen is complicated. Few distinctions have been discussed between stress concentration and geometric discontinuity. This paper presents a FE analysis of the stress concentration and geometric discontinuity of MMM signals during a tensile experiment. Section 2 presents the basic theory of the model used in this study. Then, the boundary and other details are introduced and the model is verified by experiment data in Section 3. In Section 4, the study performed to reveal the different effects of geometric discontinuity and stress concentration is discussed in detail. Finally, the conclusions are presented in Section 5.

2. Basic Theory

2.1. Magneto-mechanical model

The magnetic field in space can be described by Maxwell's magnetic equations.

$$\nabla \times \boldsymbol{H} = \boldsymbol{J} \tag{1a}$$

$$\nabla \cdot \boldsymbol{B} = 0 \tag{1b}$$

where $\boldsymbol{H}$ is the intensity of the magnetic field, $\boldsymbol{J}$ is the current density, and $\boldsymbol{B}$ is the magnetic flux density.

In the absence of free current, $\boldsymbol{J}$ equals zero. The governing equations can be written as follows by transforming Maxwell's equations with the use of the magnetic scalar potential (φ_{m}).

$$\nabla^2 \varphi_m = \nabla \cdot \mathbf{M}, \text{ in material} \tag{2a}$$

$$\nabla^2 \varphi_m = 0, \text{ in air} \tag{2b}$$

where φ_{m} is defined by $\boldsymbol{H} = -\nabla \cdot \varphi_m$.

On the interface of two different materials, the following boundary conditions are satisfied:

$$\varphi_m|_{air} = \varphi_m|_{material}, \tag{3a}$$

$$\left.\frac{\partial \varphi}{\partial_n}\right|_{air} - \left.\frac{\partial \varphi}{\partial_n}\right|_{material} = \boldsymbol{M} \cdot \boldsymbol{n}, \tag{3b}$$

where **n** is the outside unit vector normal to the surface of the ferromagnetic material.

The divergence of magnetization ($\nabla \cdot \mathbf{M}$) is the magnetic source. Then, the magnetic field distribution on the ferromagnetic material surface is determined by the source and boundary conditions.

The magnetization caused by stress is described as a magnetostriction constitutive relation. The magnetization of the material is dominated by an effective field, $\boldsymbol{H}_{\mathrm{e}}$, which can be expressed as

$$\boldsymbol{H}_e = \boldsymbol{H} + \alpha \boldsymbol{M} + \boldsymbol{H}_\sigma \tag{4}$$

where α quantifies the amount of domain coupling, and $\boldsymbol{H}_{\sigma}$ represents the equivalent magnetic field induced by the elastic stress and can be expressed as follows:

$$\boldsymbol{H}_\sigma = \frac{3\sigma}{2\mu_0} \cdot \frac{\partial \lambda}{\partial \boldsymbol{M}} \tag{5}$$

where λ is the magnetostriction and varies with the tensile stress. The exact partial differential should be determined with the measured magnetostriction curve. An empirical model can be used to simulate the relationship between magnetostriction and magnetization, and the expression that ignores the higher-order term is

$$\lambda(\sigma, \boldsymbol{M}) \approx \gamma_0 + (\gamma_{11} + \gamma_{12}\sigma)\boldsymbol{M}^2 \tag{6}$$

where γ_0, γ_{11}, and γ_{12} are stress-dependent coefficients and can be determined through fitting the measured magnetostriction curve.

Hence, the stress-induced effective field can be rewritten as

$$\boldsymbol{H}_\sigma = \frac{3\sigma}{\mu_0} \cdot (\gamma_{11} + \gamma_{12}\sigma)\boldsymbol{M}. \tag{7}$$

The anhysteretic magnetization curve, $\boldsymbol{M}_{\mathrm{an}}$, can be expressed by a modified Langevin equation as follows:

$$\boldsymbol{M}_{an} = \boldsymbol{M}_s\left(\coth\left(\frac{\boldsymbol{H}_e}{a}\right) - \frac{a}{\boldsymbol{H}_e}\right) \tag{8}$$

where $\boldsymbol{M}_{\mathrm{s}}$ is the saturation magnetization, and a is the interaction coefficient of the domain wall.

Hysteresis magnetization $\boldsymbol{M}$ can be expressed in differential form:

$$\frac{d\boldsymbol{M}}{d\sigma} = \frac{\sigma}{E\xi}(\boldsymbol{M}_{an} - \boldsymbol{M}) + c\frac{d\boldsymbol{M}_{an}}{d\sigma} \tag{9}$$

Here, $\boldsymbol{E}$ is Young's modulus, and ξ is a coefficient related to energy density.

The solution of $\boldsymbol{M}_{an}$ under different stresses can be obtained from Eqs. (4)-(8) by using a root-finding algorithm, such as the fixed point iterative method. Then, hysteresis magnetization $\boldsymbol{M}$ can also be obtained by the difference method. In this way, the nonlinear $\boldsymbol{M}$–σ relation can be calculated step by step.

The parameters of the J–A model are selected as the reported results [21]: $\gamma_{11} = -1.5 \times 10^{-18}\ A^{-2}m^2$ and $\gamma_{12} = 4.17 \times 10^{-27}\ A^{-2}m^2Pa^{-1}$.

To simplify the calculation, the constitutive relation between magnetization and stress can be fitted by a quadratic equation.

$$\boldsymbol{M} = a_0\sigma^2 + b_0\sigma + c_0$$

In this formula, coefficients a_0, b_0, and c_0 can be obtained from previously reported results [22]. Thus, a_0 is 0.555 A/mMPa^{-2}, b_0 is 0.222 A/mMPa^{-1}, and c_0 is 0.335 A/m. The residual standard deviation (measurement vs. fitting) is 0.408, and the R^2 (coefficient of determination) is 0.961. This fitting curve is applied in the FE model. Then, the magnetic field can be calculated.

2.2. FE Simulation model

The system, modeled in COMSOL Multiphysics, consists of a specimen with a groove placed in a sphere box filled with air, as shown in Fig. 1(a). The dimension of the specimen is shown in Fig. 1(b). The material of the specimen is 0.45 % carbon steel. Table 1 shows the components of this material.

The model involves two physical fields: the stress field in the solid mechanic's module and the magnetic field in the electromagnetic field module. The stress field is calculated using the mechanical equilibrium equation with the parameters from the material properties listed in Table 2.

The electromagnetic field distribution is calculated by Maxwell's magnetic equations, Eqs. (1)-(3). On the outside boundary of the surrounding air box, the magnetic scalar potential (φ_m) could be considered zero because the diameter of the air box is large enough. On the air and specimen interface, the continuous boundary conditions are satisfied. The other parameters used in the model are listed in Table 3.

The initial magnetization of each mesh in the FE model is assumed to zero. After loading, the magnetization is determined by its stress, which is calculated from the constitutive $\boldsymbol{M}$–$\boldsymbol{\sigma}$ curve. The magnetic fields generated by each mesh are merged to form the magnetic field around the specimen. Then, the MMM signals are extracted from the solution data along the scanning line as shown in Fig. 1(b).

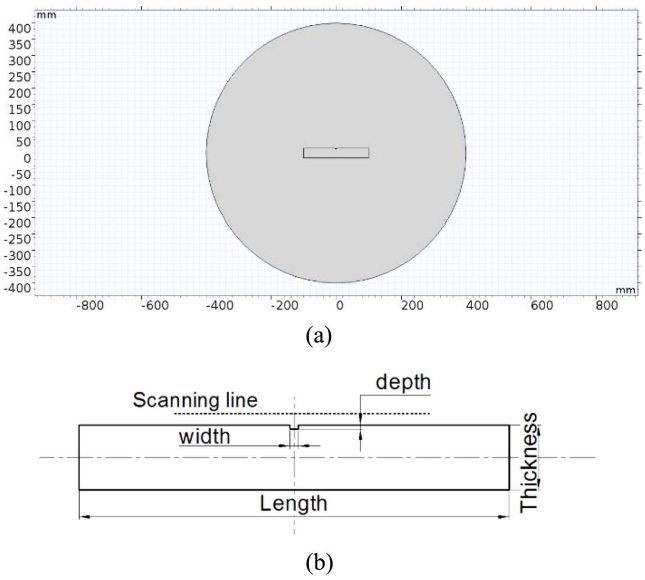

Fig. 1. Schematic of the FE model: (a) Specimen and surrounding air; (b) Geometry dimension of the specimen with a groove.

3. Experiments

Experiments were carried out to verify the simulation model. The specimens for the verification experiments

Table 2. Parameters used in the simulation model.

	Specimen	Surrounding air
Elasticity modulus	200 GPa	/
Poisson's ratio	0.3	/

Table 3. Geometry dimensions used in the FE model.

Parameters	Range				
Width of groove (mm)	4	8	12	16	20
Depth of groove (mm)	2	3	4	5	6
Tip curvature of groove (mm)			0.5		
Length of specimen (mm)			200		
Thickness of specimen (mm)			30		
Radius of airbox (mm)			400		

Table 1. Chemical composition of 0.45 % C steel (wt %).

Material	C	Si	Mn	S	P
0.45 % C steel	0.42 %–0.50 %	0.17 %–0.37 %	0.50 %–0.80 %	≤ 0.035 %	≤ 0.035 %

were made of 0.45 % C steel. The shape and dimension of the specimens were based on the simulation model in Fig. 1(b).

The tension tests were carried out on an SDS-100 testing machine. Before the experiments, the specimens were demagnetized to eliminate the initial magnetic field caused by the initial stress. Then, the specimens were clamped vertically on the SDS-100 testing machine, with a peak capacity of 100 kN. Axial tensile loads were applied to the specimens at 10 kN increments.

During testing, the specimens were first loaded to a predetermined level and then taken off from the machine and arranged along the N-S direction on a graph paper, which was fixed on a horizontal working plane. The plane had some marked points to ensure the fixed position of each measurement. The magnetic signals were scanned by a 3-axis electronic platform with a given lift-off. The precision of the platform was 0.018 mm/300 mm. The measuring range was 0.3 m × 0.3 m × 0.4 m. The theoretical resolution of the stepper motor was 1.25 μm, and the positioning accuracy of the platform was 0.02 mm. The scanning speed was 2 mm/s. The MMM signals were measured by TSC-2M-8 along the scanning line as shown in Fig. 1(b). The probe accuracy was 1 A/m.

A preparatory experiment was performed to investigate the effect of the applied tensile stress on the surface magnetic field measurement results. A healthy specimen with no groove was tensioned with a stress increment of 10 kN until 50 kN. At each level, the magnetic field was measured.

4. Results and Discussion

4.1. Model validation

The experimental MMM signals are shown in Fig. 2. The normal components $\boldsymbol{H}_p(y)$ along the scanning line are almost linear, and the slope value of the curves increases with the stress.

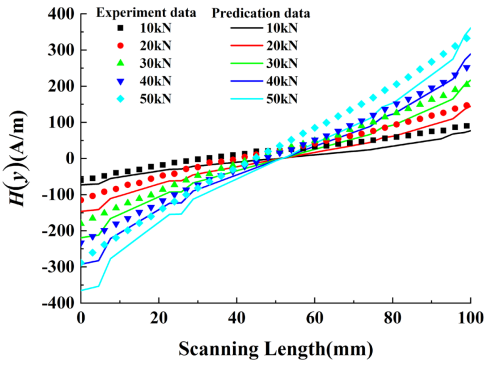

Fig. 2. Comparison of magnetic memory signals predicted by the simulation model and experiments.

Figure 2 shows that the prediction is consistent with the experimental data. Therefore, the prediction can satisfactorily describe the variation of the magnetic field of the specimen. This result also indicates that the slope of $\boldsymbol{H}_p(y)$ reflects the magnetization of the specimen, which cannot be removed as it is not only related to the specimen geometry as in Ref. [1].

4.2. Comparison of stress and magnetic distributions

Around the groove, a stress concentration zone (SCZ) is generated in the specimen when a tensile load is applied along the axis. The stress distribution is shown in Fig. 3. Only the area near the groove is plotted. Fig. 3 reveals the location of the SCZ with a maximum stress of 392 MPa and nominal stress of 111 MPa. The stress concentration factor was calculated to be 3.53, which is consistent with the analysis results of elastic mechanics. The area beyond the yield limit of the material (360 MPa) is very small, and the effect of plastic deformation on the magnetic signal can be ignored.

The magnetic flux density $\boldsymbol{B}$ distribution caused by stress is shown in Fig. 4. An abnormality of $\boldsymbol{B}$ can be observed near the groove. The maximum magnetization area is located at the bottom of the groove. And the magnetization on the side of groove is weakest, for the side is the free boundary of the stress field as shown in Fig. 3. This conclusion is completely different from the hypothesis in the magnetic charge theory that the magnetic charge is distributed on the side of the groove [19].

4.3. Comparison of geometry defect and stress distribution

The uniform magnetization provided in the SMFL method was also simulated in the same COMSOL model to investigate the impacts of the geometric discontinuity and stress distribution. The distribution is shown in Fig. 5. The magnetic field distribution is inconsistent with the stress distribution in Fig. 3, indicating that the magnetic

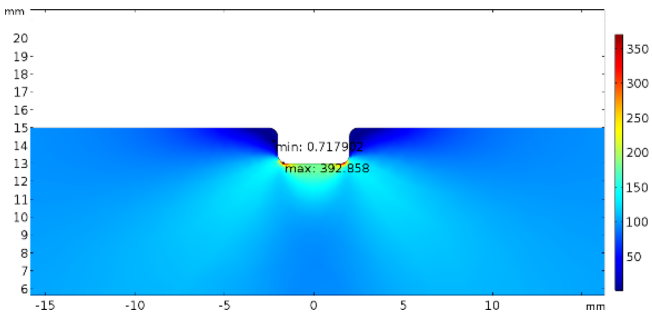

Fig. 3. Stress (Von mises) distribution with a tensile load of 20 kN.

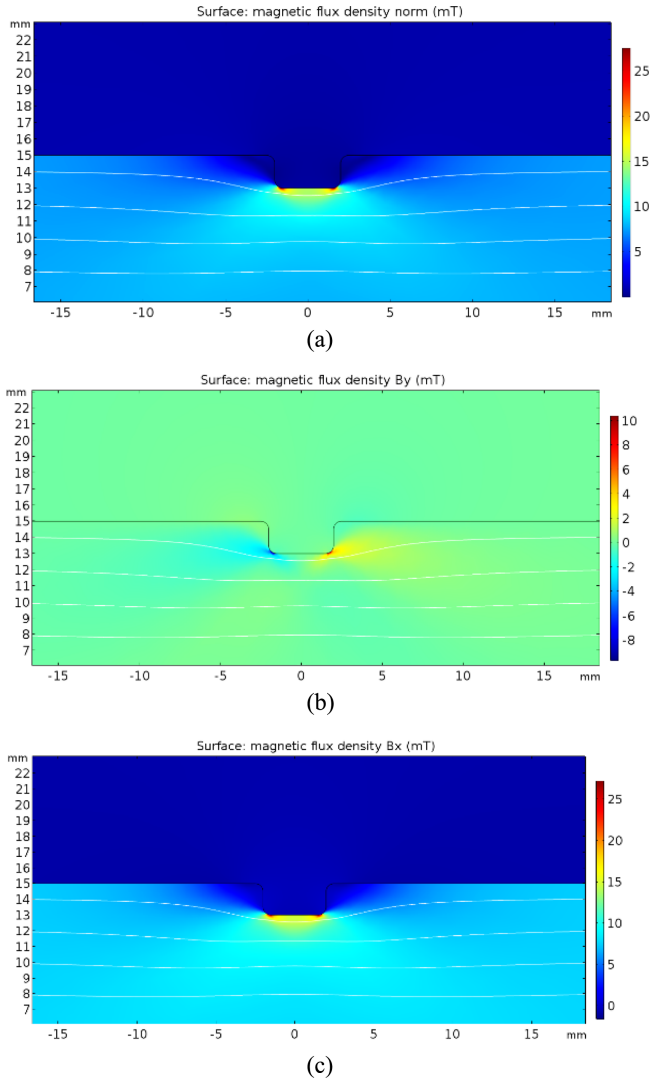

Fig. 4. Distribution of magnetic field (a) norm $\boldsymbol{B}$, (b) normal $\boldsymbol{B}_y$, and (c) tangential $\boldsymbol{B}_x$ caused by stress.

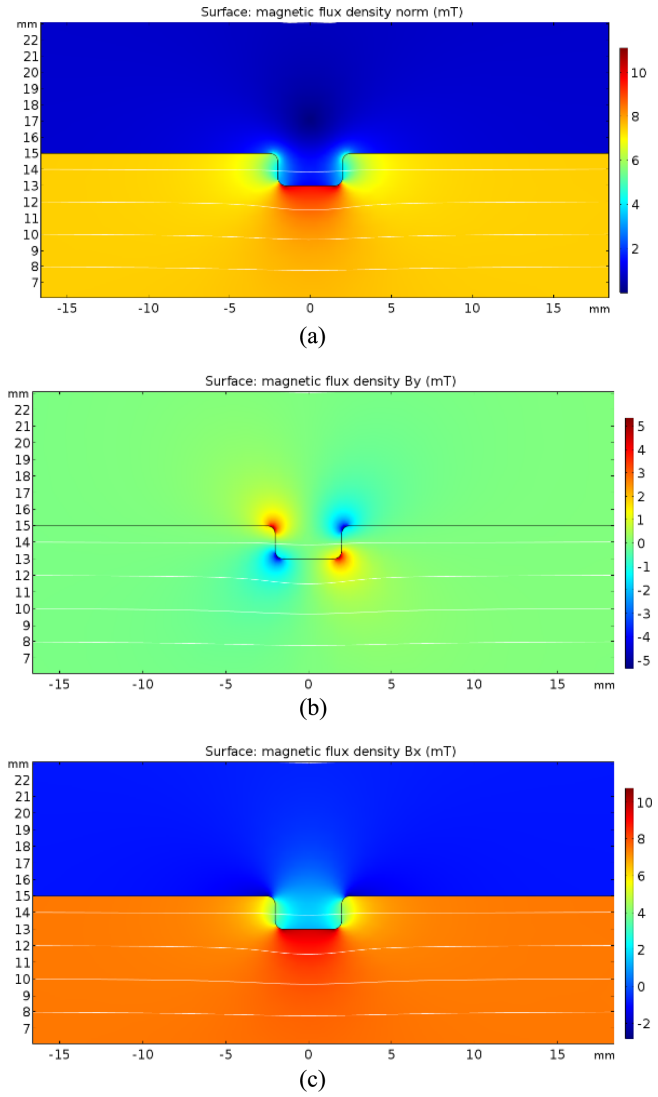

Fig. 5. Distribution of magnetic field (a) norm $\boldsymbol{B}$, (b) normal $\boldsymbol{B}_y$, and (c) tangential $\boldsymbol{B}_x$ caused by a geometric defect.

distribution is more complicated than and different from the stress distribution due to the geometry discontinuity.

To understand the impact of the geometric defect and stress distribution of the groove, we plot the curves of the tangential signals $\boldsymbol{H}_x$ and normal signals $\boldsymbol{H}_y$ variation along the scanning line in Fig. 6. As expected, the $\boldsymbol{H}_x$ signal shows a unipolar behavior, while the $\boldsymbol{H}_y$ signal shows a bipolar behavior. The peak value of the $\boldsymbol{H}_x$ component corresponds to the location of the groove. This behavior is consistent with the previous experimental observation [16]. Furthermore, the two types of curves have the same trend. It can be seen that an obvious decrease can be observed for the stress magnetization when compared to the geometric discontinuity, and the abnormality due to geometric discontinuity is even stronger than those due to stress concentration, which indicates that the stress concentration may decide the weak magnetic leakage field.

4.4. Analysis and discussion of the influence of geometry and stress

To present quantitative results about the signals, two characteristic parameters are defined, namely, the peak-peak amplitude $S_{p\text{-}p}$ and peak-peak width $w_{p\text{-}p}$ of the normal component, as shown in Fig. 7.

Figure 8 shows the variation of $S_{p\text{-}p}$ with the increase of the groove depth. The groove depth has a remarkable impact on the magnetic field amplitude $S_{p\text{-}p}$ for both stress concentration and geometric discontinuity. However, the value of $S_{p\text{-}p}$ and its increment caused by geometry discontinuity are distinctly higher than those by stress con-

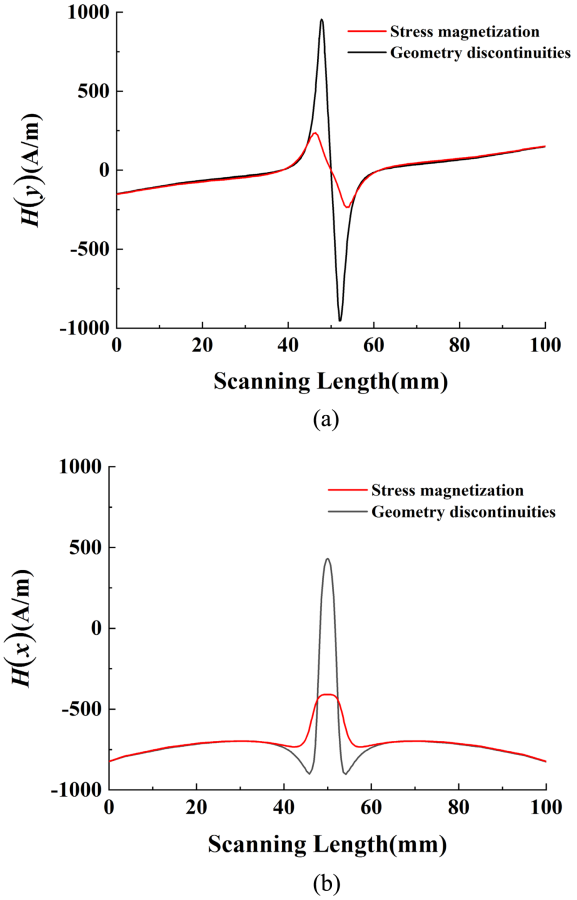

Fig. 6. Comparison of magnetic memory signals due to geometry discontinuity and stress magnetization: (a) normal signals; (b) tangential signals.

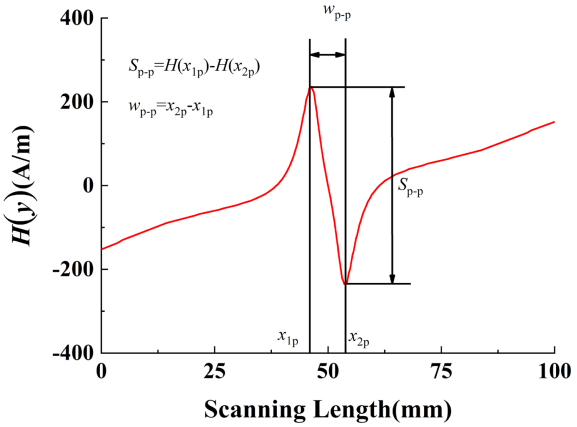

Fig. 7. Curves and parameters of the normal component.

centration.

Furthermore, S_{p-p} decreases with the increase of width under a constant depth on the condition of stress concentration. However, it increases with the increase of width on the condition of geometric discontinuity. This is because

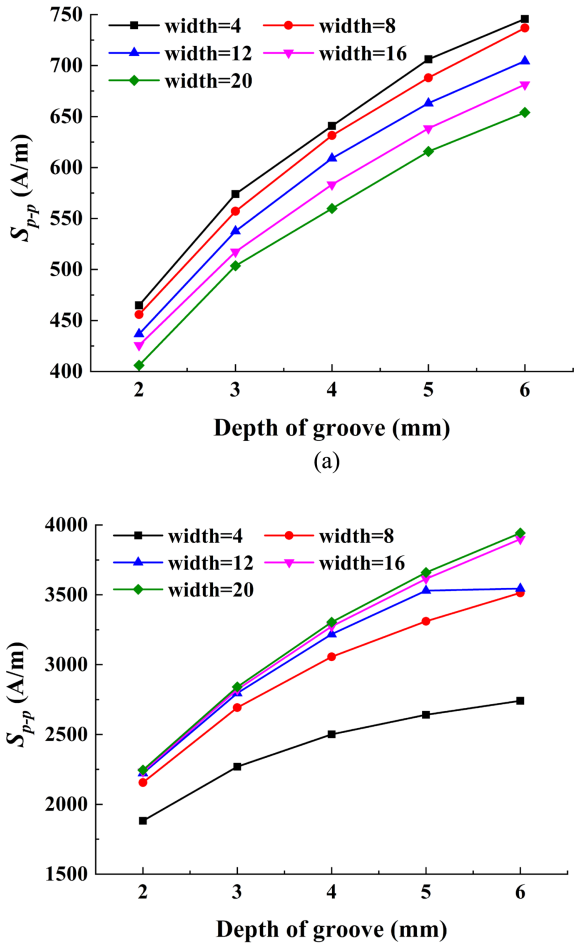

Fig. 8. Variation of S_{p-p} with different groove depths by (a) stress concentration and (b) geometric discontinuity.

that, with the increase of the width, the slope of normal component of MMM signal of the entire specimen weakens the characteristic parameters S_{p-p} on the condition of stress concentration. However, on the condition of geometric discontinuity, for the value of S_{p-p} is much larger, the slop of MMM signal of the entire specimen can be ignored, which has little effect on the variation of S_{p-p}.

Figure 9 shows the w_{p-p} variation with the increase of the groove depths. The groove depth has a slight influence on the peak-peak width w_{p-p} due to the stress concentration, as shown in Fig. 9(a). In contrast, the groove depth has little influence on geometric discontinuity.

In the traditional MFL method, magnetic charges are assumed to be concentrated in the walls of the breaking defect. Thus, the w_{p-p} remains constant with the depth. However, the stress is released in the walls of the groove, and the main reason for the magnetic leakage field is the magnetization caused by stress concentration at the bottom of the groove. Since the measured signals come

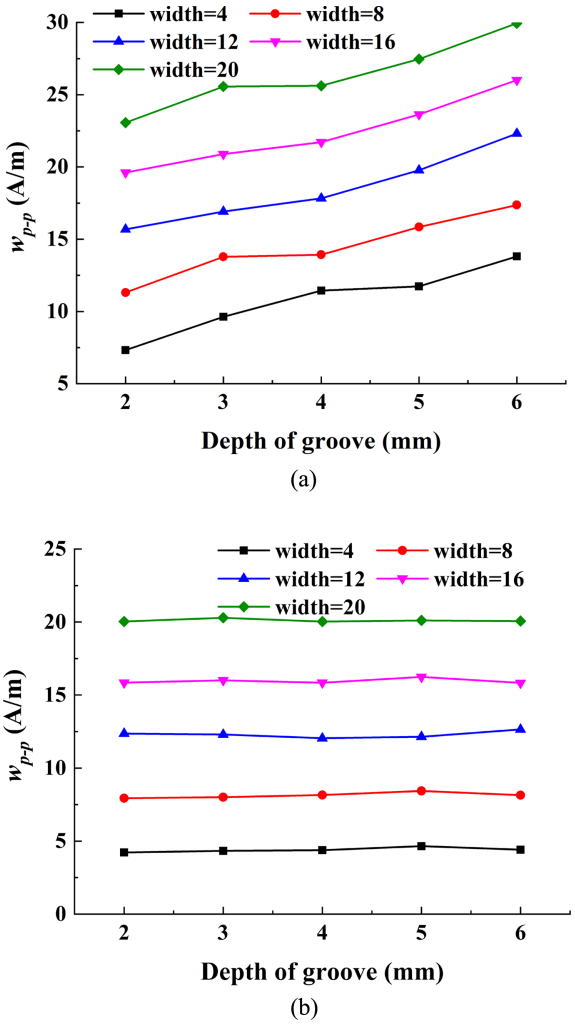

Fig. 9. Variation of w_{p-p} with different groove depths by (a) stress concentration and (b) geometric discontinuity

from the surface of the specimen, w_{p-p} can be seen as a far field characteristic of a defect in this case. Previous studies indicated that the peak-peak width increases with the increase of the lift-off value, when the lift-off value is not very small [23], which explains why w_{p-p} increases with the increase of depth.

The numerical results show that stress concentration and geometric discontinuity can also affect the MMM signal and have a similar variation trend. In this study, maximum stress was observed at the bottom of the groove. Meanwhile, the free boundary condition releases the stress concentration of surface of the defect. This indicate that the geometry discontinuity is the main factor that determines the distribution of the magnetic field. The non-uniform magnetization induced by stress weakens the magnetic leakage field. It also reduces the peak-peak amplitude S_{p-p} and increases the peak-peak width w_{p-p}. The proposed simulation model further explains the complex relation of stress concentration and geometry shape and promotes the application of the MMM.

5. Conclusions

In this work, the MMM model based on the magneto mechanical effect was introduced and verified. A multi-physics FE model was adopted for a grooved specimen to study the effect of geometric discontinuity and stress concentration on the MMM signals. The quantitative distinction was investigated. The following conclusions are drawn from this study:

(1) This model can simulate the magnetic abnormality of geometric discontinuity and stress concentration. The results of this research would be useful for the reliable and accurate damage estimation of engineering structures using the MMM technique.

(2) The calculation results show that the magnetization on the wall of the groove is the weakest and that on the bottom of the groove is the maximum. These results are inconsistent with the magnetic charge theory of the traditional MFL method.

(3) Geometric discontinuity is the main reason of the magnetic leakage field. The free boundary condition releases the stress concentration of the defect. The non-uniform magnetization induced by stress weakens the magnetic leakage field. It reduces the peak-peak amplitude S_{p-p} and increases the peak-peak width w_{p-p}.

(4) Under stress magnetization, the signal amplitude decreases considerably. Although the stress distribution weakens the magnetic leakage field, the signal characteristic can still be used to evaluate the defect and the stress. Thus, MMM is a potential method for stress distribution assessment.

Acknowledgements

This work was financially supported by the National Natural Science Foundation of China (Grant No. 51675155, 51722502).

References

[1] Z. Li, S. Dixon, P. Cawly, R. Jarvis, P. B. Nagy, and S. Cabeza, NDT & E Int. **92**, 136 (2017).
[2] A. A. Doubov, Weld World **41**, 196 (1998).
[3] L. Q. Zhong, L. M. Li, and X. Chen, IEEE T. Magn. **49**, 1128 (2013).
[4] S. K. Ren, X. Z. Ren, Z. X. Duan, and Y. W. Fu, NDT & E Int. **103**, 77 (2019).
[5] M. Moonesan and M. Kashefi, J Magn. Magn. Mater.

460, 285 (2018).
[6] M. Roskosz and M. Bieniek, NDT & E Int. **45**, 55 (2012).
[7] Z. Usarek, B. Augustyniak, and M. Augustyniak, IEEE Trans. Magn. **50**, 6201204 (2014).
[8] H. Huang, L. Zhao, and B. Xiong, D. Zhou, Z. Qian, and Z. Liu, J. Nondestuct Eval. **39**, 27 (2020).
[9] G. J. Jung, J. S. Seo, and Y. W. Park, J. Magn. **24**, 281 (2019).
[10] H. H. Huang, S. L. Jiang, R. J. Liu, and Z. F. Liu, J. Nondestruct. Eval. **33**, 407 (2014).
[11] M. Augustyniak and Z. Usarek, J. Nondestruct. Eval. **34**, 1 (2015).
[12] L. Wu, K, Yao, P. Shi, B Zhao, and Y. Wang, NDT & E Int. **109**, 102178 (2020).
[13] Z. D. Wang, K. Yao, B. Deng, and K. Q. Ding, NDT & E Int. **43**, 513 (2010).
[14] K. Yao, K. Shen, Z. D. Wang, and Y. S. Wang, J. Magn. Magn. Mater. **354**, 112 (2014).
[15] C. Shi, S. Dong, B. Xu, and P. He, NDT & E Int. **43**, 8 (2010).
[16] M. Roskosz and M. Bieniek, NDT & E Int. **45**, 55 (2012).
[17] P. Shi, J. Magn. Magn. Mater. **512**, 166980 (2020).
[18] P. Zhang, P. Shi, K. Jin, and X. Zheng, J. Appl. Phys. **125**, 233901 (2019).
[19] P. P. Shi, J. Ke, and X. J. Zheng, IEEE Trans. Magn. **54**, 1 (2018).
[20] P. P. Shi, K. Jin, and X. Zheng, Int. J. Mech. Sci. **124–125**, 229 (2017).
[21] P. Wang, Y. Gao, G. Y. Tian, and H. Wang, NDT & E Int. **64**, 7 (2014).
[22] D. C. Jiles, J. B. Thoelke, and M. K. Devine, IEEE Trans. Magn. **28**, 27 (1992).
[23] C. Mandache and L. Clapham, J. Phys. D Appl. Phys. **36**, 2427 (2003).